Monthly Notices
of the
ROYAL ASTRONOMICAL SOCIETY

Mon. Not. R. Astron. Soc. **416,** 522–530 (2011) doi:10.1111/j.1365-2966.2011.19064.x

GMRT observations of NGC 2997 and radio detection of the circumnuclear ring

J. Kodilkar,[1⋆] N. G. Kantharia[1] and S. Ananthakrishnan[2]

[1]*National Centre for Radio Astrophysics, Tata Institute of Fundamental Research, Post Bag 3, Ganeshkhind, Pune 411 007, India*
[2]*Department of Electronic Science, Pune University, Pune 411 007, India*

Accepted 2011 May 12. Received 2011 April 29; in original form 2010 July 9

ABSTRACT

We present high-resolution, high-sensitivity radio continuum observations of the nearby spiral galaxy NGC 2997 at 332, 616 and 1272 MHz using the Giant Metrewave Radio Telescope (GMRT). The integrated spectrum of this galaxy has a spectral index of −0.92 ($S_\nu \propto \nu^\alpha$) and we place an upper limit to the thermal fraction at 1272 MHz of ∼ 10 per cent. Our multifrequency study shows a relatively flat spectrum source ($\alpha \sim -0.6$) at the centre of the galaxy. This leads to the radio detection of a circumnuclear ring in the high-resolution map at 1272 MHz. We detect five hotspots in the ring, with an average star formation rate of $\sim$0.024 $M_\odot$ yr^{-1}, a median supernova (SN) rate of $\sim$0.001 yr^{-1} and luminosity of 10^{20} W Hz^{-1}. We estimate an equipartition field in the central nuclear region of diameter ∼750 pc to be about 30 μG. We also report several interesting features along the spiral arms. In this paper, we present the low-frequency radio continuum maps, the spectral index distribution, the circumnuclear ring and the derived physical properties.

Key words: galaxies: individual: NGC 2997 – galaxies: nuclei – radio continuum: galaxies.

1 INTRODUCTION

NGC 2997 is an interesting grand design spiral galaxy of type SAB(rs)c located in the loose galaxy group LGG 180 (Garcia 1993). The disc inclination is ∼40° (Milliard & Marcelin 1981) and the southern part of the disc is closer to us (Peterson 1978). We assume a distance of 13.8 Mpc (Tully 1988) to NGC 2997 and note that 1 arcmin corresponds to a linear scale of ∼4.0 kpc. The basic data on NGC 2997 are listed in Table 1.

The photometric and morphological analysis of this galaxy shows the presence of a normal nucleus surrounded by several H II regions known as 'hotspots' (Pastoriza 1975). Further investigations in optical (Meaburn & Terrett 1982), ultraviolet (Maoz et al. 1996) and near-infrared (Elmegreen et al. 1999) have detected a circumnuclear star-forming ring in NGC 2997. The study of such a ring is significant in terms of understanding the gas transport to the inner regions of the galaxy and its association with any possible nuclear activity. NGC 2997 also shows several bright knots of emission along its arms. These knots are young star clusters with typical masses of $\sim 5 \times 10^4$ $M_\odot$ (Grosbøl, Dottori & Gredel 2006). This galaxy also hosts two giant H II regions which show supersonic velocity dispersion caused by an intense starburst (Firpo, Bosch & Morrell 2005). The galaxy that is part of the H I brightest galaxy catalogue of the southern sky derived from HIPASS has an H I mass of $\sim 4.2 \times 10^9$ $M_\odot$ and half-power linewidth of 254 km s^{-1} (Koribalski et al. 2004).

NGC 2997 has been extensively studied in radio wavelengths shorter than 20 cm by Han et al. (1999) and Men & Han (2005). To the best of our knowledge, this galaxy has not been studied at longer wavelengths ($\lambda > 20$ cm). Since the non-thermal spectrum of synchrotron radiation is dominant at low frequencies, the Giant Metrewave Radio Telescope (GMRT) observations at metre-wavelengths with a high angular resolution and high sensitivity can reveal many significant features of NGC 2997 due to its moderate inclination such as smooth synchrotron emission from the disc, morphological structure of spiral arms, nucleus and compact H II regions. The spectral index distribution study of NGC 2997 could be useful for identification of giant H II regions.

The low radio frequency spectrum of the galaxy is important in obtaining the non-thermal spectral index of the galaxy which can then be used to separate the thermal and non-thermal contributions to the observed spectrum. Moreover, the non-thermal luminosities at low frequencies can be used to estimate the supernovae rate (yr^{-1}), average star formation rate ($M_\odot$ yr^{-1}), production rate of the Lyman continuum photons (s^{-1}) etc. for the galaxy.

In this paper, we present radio continuum observation of NGC 2997 using the GMRT (Swarup et al. 1991; Ananthakrishnan 2005) at 332, 616 and 1272 MHz. Section 2 describes the observations and the data reduction procedure. Section 3 presents the total intensity

⋆E-mail: jkodilkar@gmail.com

Table 1. Basic data on NGC 2997[†].

Optical centre (J2000)	$09^h45^m38\overset{s}{.}8\ -31^\circ11'28''$
Morphological type[‡]	SAB(rs)c
Major diameter (arcmin)	8.9
Minor diameter (arcmin)	6.8
Distance ($H_0 = 75\,\mathrm{km\,s^{-1}\,Mpc^{-1}}$)	13.8 Mpc
Magnitude (visual)	10.06
Inclination angle (°)	40
Heliocentric radial velocity ($\mathrm{km\,s^{-1}}$)	1088 ± 2

[†]Reference: NASA/IPAC Extragalactic Data base (NED).
[‡]de Vaucouleurs et al. (1991).

maps and the morphological details of radio continuum features of NGC 2997. In Section 4, we discuss the total emission spectrum of the galaxy, the spectral index map derived between 1272 and 332 MHz, and the circumnuclear ring. The last section summarizes the paper.

2 OBSERVATIONS AND DATA REDUCTION

We had a total of three observing sessions on NGC 2997 using the GMRT synthesis array at each of the three frequency bands 332, 616 and 1272 MHz, respectively. Observing sessions were conducted in the period from 2003 to 2004 using the standard spectral line mode of the GMRT digital correlator which gives visibility data of 16-MHz bandwidth across 128 channels for two polarizations. The observational parameters are summarized in Table 2. The raw visibility data were converted to FITS and analysed using standard AIPS.[1]

The VLA flux density calibrators, 3C147 and 3C286, were used as flux density reference to scale the flux densities of phase calibrators and the target source. To correct the ionospheric and instrumental gain variations, the phase calibrator 0837-198 was observed for 6 min during every 25 min of observation of the target source. The flux density values of phase calibrators obtained using the task GETJY are given in Table 2. The flux density calibrators were also used for bandpass calibration. To avoid the bandwidth smearing effect, the bandpass-calibrated data at 616- and 1272-MHz bands were collapsed to five channels each of ∼2.75-MHz bandwidth by averaging every 22 channels. At 332 MHz, 10 channels each of ∼1.25-MHz bandwidth formed from RFI free band by averaging every 10 channels. The expected error bars in flux density scale for the GMRT observations are $\lesssim$10 per cent.

First, a low-resolution map of ∼45 arcsec was made using 'uvtaper' at each observing frequency and the entire primary beam was imaged. We also used varying tapers to generate maps of different angular resolutions which can be compared at the different frequencies. There were two to three strong point sources near the edge of the primary beam at each frequency with peak flux 10–12 times stronger than the peak flux on the object. These sources were removed using the task UVSUB.

Wide-field imaging was used at 616 and 332 MHz. The number of facets used for imaging NGC 2997 at 616 and 332 MHz were 13 and 22, respectively (obtained using SETFC task in AIPS). No self-calibration was done at 1272 MHz. At other frequencies, the visibility data sets were first phase self-calibrated using only strong point sources near or within the inner quarter of the primary field. After two to three iterations of phase self-calibration using only point sources, the source model obtained by cleaning up to the rms noise level of the map was included in self-calibration. At 332 and 616 MHz, it took about four to six iterations to get a good convergence of self-calibration resulting in improved dynamic range maps. All the facets were combined and primary beam correction applied using the FLATN task to produce a map at each observing frequency.

3 OBSERVATIONAL RESULTS

3.1 Total intensity maps

We made total intensity maps of the object with angular resolution ranging from 45 to 3 arcsec. Whenever possible, the total intensity maps at different observing frequencies were made with a similar angular resolution by using the uv-tapering function in the task 'IMAGR'. Fig. 1 shows the total intensity maps of NGC 2997 at 1272, 616 and 332 MHz at a resolution of 15 arcsec overlaid on the optical Digitized Sky Survey image. The uv-tapering and weighting functions used while mapping the object are given in Table 3.

The multifrequency total intensity GMRT maps in Fig. 1 show about six common radio continuum features of NGC 2997. These discrete features are labelled by numbered tags in Fig. 1(a). In Table 4, we summarize their positions, size, observed flux densities, etc. The peak positions of the discrete features listed in Table 4 match within the median errors of $\Delta\mathrm{RA} \sim \pm0\overset{s}{.}22$ and $\Delta\mathrm{Dec.} \sim \pm2$ arcsec. The summary of radio continuum emission features seen in NGC 2997 is as follows.

(i) The radio disc in the GMRT low-resolution images has an extent of ∼6.5 arcmin by 8 arcmin which is comparable to the optical extent. The extent of radio emission in the low-resolution map at 1272 MHz is comparable to the NVSS grey-scale image (Condon et al. 1998) as shown in Fig. 2.

(ii) All our total intensity maps show the compact bright nucleus, centred at, RA = $09^h45^m38\overset{s}{.}76$; Dec. = $-31^\circ11'26\overset{''}{.}60$ (J2000). The uncertainties in RA and Dec. are $\sim0\overset{s}{.}03$ and ∼0.4 arcsec, respectively. The radio peak position coincides with the values given by Han et al. (1999), Men & Han (2005) and also the optical centre (see Table 1). At a first glance, the intense unresolved nucleus at 15-arcsec resolution (Fig. 1) appears like an active galactic nuclei (AGN).

(iii) The radio continuum emission associated with both the spiral arms is clearly detected in all the maps shown in Fig. 1. There is an intense ridge of emission along the northern spiral arm as compared to the southern arm.

(iv) No radio emission is detected in the northern part of the southern spiral arm near the region at RA = $9^h45^m32\overset{s}{.}8$; Dec. = $-31^\circ10'$ (labelled 'GAP' in Fig. 1a). This region is bluer in the optical image, suggesting a young star-forming complex. This gap has also been noted in the VLA total intensity maps at λ20, 18, 6 cm and in the polarized intensity maps at λ6 and 13 cm (Han et al. 1999; Men & Han 2005).

(v) A bright compact source (component 2) is seen in all our maps of NGC 2997 at RA = $09^h45^m39\overset{s}{.}6$; Dec. = $-31^\circ08'51\overset{''}{.}1$, in the north of the galaxy. No discrete optical counterpart is seen for this source.

(vi) All the maps in Fig. 1 show an intense region (component 3) in the northern spiral arm, near RA = $09^h45^m45^s$; Dec. = $-31^\circ10'33''$. This compact region is coincident with the giant H II

[1] Astronomical Image Processing System, distributed by the National Radio Astronomy Observatory, http://www.aips.nrao.edu. The NRAO is a facility of the National Science Foundation operated under cooperative agreement by Associated Universities, Inc.

Table 2. Observation table.

	Observing band (MHz)	332	616	1272
1.	Date	2004 February 24	2003 January 21	2003 August 16
2.	Correlator used (USB/LSB)[a]	USB	USB	LSB
3.	On source time (h)[b]	5	4	3
4.	Receiver bandwidth (MHz)	16	16	16
5.	Number of working antennas[c]	27	24	28
6.	Shortest spacing (kλ)	0.06	0.120	0.250
		∼55 m	∼60 m	∼58 m
7.	Longest spacing (kλ)	27	40	101
		∼25 km	∼20 km	∼24 km
8.	Largest visible structure[d]	∼19 arcmin	∼12 arcmin	∼8 arcmin
9.	Flux density calibrator (s)	3C147, 3C286	3C147, 3C286	3C147, 3C286
	Flux density in Jy[e]	52.69, 25.96	38.26, 21.07	23.69, 15.48
10.	Phase calibrator (s)	0837-198, 0902-142	0837-198	0837-198
	Flux density in Jy[f]	13.3 ± 0.4, 4.3 ± 0.1	8.7 ± 0.08	4.6 ± 0.1

[a]USB-Upper side band, LSB-Lower side band. [b]Total observation time on the object before editing. [c]Maximum number of antenna operational at any time during the observation. [d]Corresponding to the shortest spacing present in our data. [e]Set by SETJY task: Using VLA (1999.2) or Reynolds (1934-638) coefficients. [f]Flux density and error from GETJY.

region identified by Firpo et al. (2005) using high-resolution optical spectra (λ3726–7136 Å). Apart from this, a prominent north-east discrete component (labelled 'NE Comp.') is seen in Figs 1(a) and (b), positioned at RA = $09^{\rm h}45^{\rm m}49\overset{\rm s}{.}28$, Dec. = $-31^\circ10'11\overset{''}{.}02$ (J2000) and lying roughly above the northern ridge. This component appears to be a flat spectrum source since it is barely detected in the 332 MHz map (Fig. 1c).

Global radio continuum properties

The integrated flux densities given in Table 5 are obtained by integrating the region above 3σ contour in the low-resolution maps (45 arcsec). The measured spectral power ranges from $\sim 7.9 \times 10^{21}\,{\rm W\,Hz^{-1}}$ at 1272 MHz to $24.4 \times 10^{21}\,{\rm W\,Hz^{-1}}$ at 332 MHz. At 1.4 GHz, normal galaxies range in power from $L \lesssim 10^{18}$ to $\sim 10^{23}\,{\rm h^{-2}\,W\,Hz^{-1}}$ where $h \equiv H_0/(100\,{\rm km\,s^{-1}\,Mpc^{-1}})$ (Condon 1992). The global spectral index values given in Table 5 indicate that the spectrum flattens at the lower frequencies. The total emission spectrum of many normal spiral galaxies with moderate surface brightness are known to show a break in the range from 0.1 to 1 GHz. One of the reasons for this is possibly free–free absorption by the cool ($T_{\rm e} < 1000$ K) ionized gas filling a large fraction of the radio-emitting volume (Israel & Mahoney 1990). On the other hand, the break could be due to the propagation effects of relativistic electrons and the subsequent energy losses (Hummel 1991; Pohl, Schlickeiser & Hummel 1991).

The radio-selected samples of normal galaxies are characterized by the far-infrared (FIR)/radio flux density ratios (Condon 1992). Helou, Soifer & Rowan-Robinson (1985) defined the parameter q as a logarithmic measure of the FIR/radio flux density ratio. For more general comparisons, the $\hat{q}_{\rm FIR}$ is defined as $\hat{q}_{\rm FIR} = \log\{{\rm S}_\nu({\rm FIR})/[{\rm S}_\nu({\rm rad}) \times (\nu_{\rm rad}/1.4\,{\rm GHz})^{-\alpha})]\}$ (Fitt et al. 1992), where α is the radio spectral index ($S_\nu \propto \nu^\alpha$). The spectral index for the observed GMRT data is -0.79 ± 0.07. From the *IRAS* surveys (Fitt et al. 1992) at 60 and 100 μm the flux densities of NGC 2997 are 32.28 and 85.14 Jy, respectively. Using the *IRAS* FIR flux density measurements and integrated flux densities measured with the GMRT, the derived $\hat{q}_{\rm FIR}$ parameter is $\sim 2.19 \pm 0.03$, which is close to the median for spiral galaxies at 1.4 GHz, i.e. $\hat{q}_{\rm FIR} \approx 2.30$ with the rms scatter $\sigma_{\hat{q}} \lesssim 0.2$ (Helou, Soifer & Rowan-Robinson 1985; Condon & Broderick 1988; Condon, Frayer & Broderick 1991). The spectral power and FIR/radio flux density ratio found at our observing frequencies confirm that NGC 2997 is a normal spiral galaxy.

4 DISCUSSION

4.1 The observed radio spectrum and SFR

Integrated flux densities of NGC 2997 obtained using the GMRT and other published data from 0.33 to 8.46 GHz are listed in Table 6. A single power law ($S_\nu \propto \nu^\alpha$) with $\alpha = -0.92 \pm 0.04$ gives the best fit to the radio spectrum from 0.33 to 5 GHz (Fig. 3). A value of $\alpha = -1.10 \pm 0.07$ is quoted by Men & Han (2005) for the radio spectrum from 1.43 to 8.46 GHz. Niklas, Klein & Wielebinski (1997) analysed the radio continuum spectra of 74 galaxies to separate the thermal and the non-thermal radio emission. The mean value obtained for non-thermal spectral index is $\langle\alpha_{\rm nt}\rangle = -0.83 \pm 0.02$. They also studied the correlation of the morphological type and non-thermal spectral index and found that spiral galaxies of type Sc show $\alpha_{\rm nt}$ to be in the range of -0.8 to -1.05. Spectral index of NGC 2997, which is an Sc galaxy, lies in the above range. The flatter spectrum $\alpha = -0.79 \pm 0.07$ for the GMRT data at the lower frequencies compared to the wide-band spectral index value could suggest a break in the spectrum at $\nu < 1$ GHz. However, the change in α is only $\sim 2\sigma$ and needs to be confirmed with data at a still lower ν.

Condon & Yin (1990) estimated a global thermal fraction for most of the normal galaxies as $S/S_{\rm th} \sim 1 + 10(\frac{\nu}{\rm GHz})^{(0.1-|\alpha_{\rm nt}|)}$, where S is the total flux density and $S_{\rm th}$ is the flux density due to the thermal component. Taking $\alpha_{\rm nt} = -0.79$, thermal fractions derived at 1272, 616 and 332 MHz are ∼10, 6 and 4 per cent, respectively, of the measured total flux density value at each observing band. The derived thermal fraction at 1.2 GHz agrees with the obtained mean value of thermal fraction at 1 GHz for 74 galaxies by Niklas et al. (1997) which is $\langle f_{\rm th}^{\rm 1GHz}\rangle = 0.08 \pm 0.01$. The average thermal fraction at 1.4 GHz in normal galaxies is $\lesssim 10$ per cent (Kennicutt 1983b; Condon & Yin 1990).

The standard method applied here to derive the thermal fraction using the constant non-thermal spectral index is simplistic. Tabatabaei et al. (2007b) derived the thermal radio continuum in the galaxy M33 from the extinction-corrected Hα map instead of

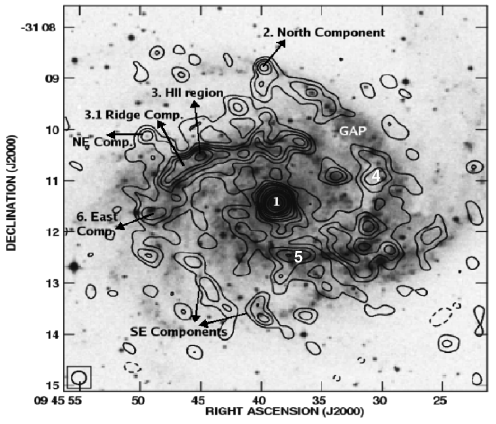

(a)

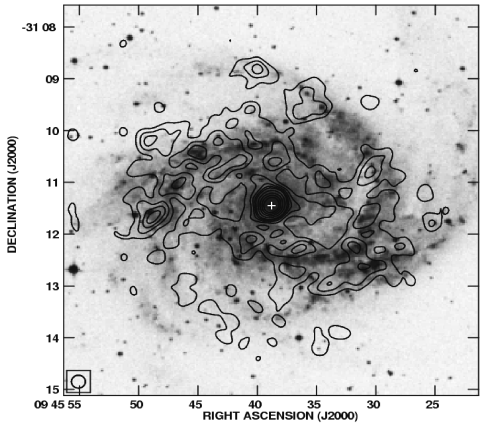

(b)

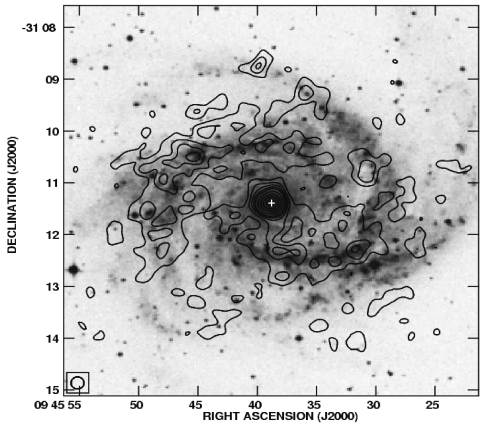

(c)

Figure 1. The total intensity maps of NGC 2997 with a resolution of 15 arcsec at 1272, 616 and 332 MHz. (a) The 1272 MHz radio contour map superimposed on the optical Digitized Sky Survey image. The six discrete radio continuum features detected at three wavebands are labelled with numbers. The peak brightness is 21 mJy beam^{-1}. The rms σ is 0.3 mJy per beam area, the beam is depicted at the bottom-left corner. The contours are at $(-3, 3, 5, 7, 9, 11, 15, 20, 25, 30, 40, 50, 60, 70) \times \sigma$. (b) The 616 MHz radio contour map overlaid on the DSS optical image. The radio peak position of the nucleus is marked as a plus sign. The peak brightness is 28.4 mJy beam^{-1}. The rms σ is 0.6 mJy per beam area, the beam size is depicted at the bottom-left corner. Contours: $(-3, 3, 5, 7, 9, 11, 15, 20, 25, 30, 40) \times \sigma$. (c) The 332-MHz radio contour map overlaid on the DSS optical image. The radio peak position of the nucleus is marked as a plus sign. The peak brightness is 40.9 mJy beam^{-1}. The rms σ is 1 mJy per beam area, the beam size is shown at the BLC. Contours: $(-3, 3, 5, 7, 9, 11, 15, 20, 25, 30, 40) \times \sigma$.

using a constant α_{nt} across the galaxy. They found that the thermal fraction of M33 at 3.6 cm using the new method is 23 ± 14 per cent lower than that found by assuming a constant α_{nt} across the galaxy. However, Tabatabaei et al. (2007b) note that the thermal fraction derived from the radio-integrated spectrum of M33 using the standard method and the new method agree. Hence, the assumption of a constant non-thermal spectral index to derive the thermal fraction is reasonable when the integrated spectrum is used.

Considering the small value of the thermal fraction in the total emission of NGC 2997 at low frequencies, we assume that the spectral power given in Table 5 is mostly non-thermal. We estimate the supernova rate (yr^{-1}) in NGC 2997 from the non-thermal luminosity (Condon & Yin 1990). The estimated supernova rate for the disc and nuclear region is about $\sim$0.08 and $\sim$0.01 yr^{-1}, respectively. In order to compare the supernova (SN) rate per kpc^2, we assumed a diameter $\sim$1.3 and $\sim$24.5 kpc for the nucleus and the disc, respectively. The SN rate per kpc^2 for the nucleus and the whole disc is about $\sim 8 \times 10^{-3}$ yr^{-1} kpc^{-2} and $\sim 0.14 \times 10^{-3}$ yr^{-1} kpc^{-2}, respectively. If we assume a filling factor of $\sim$0.7 for the disc, the SN rate for the disc is about $\sim 0.2 \times 10^{-3}$ yr^{-1} kpc^{-2}, i.e. the nuclear region has an SN rate which is 40 times higher than the rate in the disc.

The tight correlation between the radio continuum intensities and the FIR luminosities is known to be linear over a wide range in star formation rate (SFR) from normal spirals to the most intense starbursts (Lacki, Thompson & Quataert 2010). Roy et al. (1998) found that Seyfert galaxies with radio-quiet cores follow the linear radio–FIR correlation similar to normal galaxies. NGC 2997 is a late-type spiral galaxy and having no obvious companion (Milliard & Marcelin 1981). The resultant steep spectral index $\alpha = -0.92 \pm 0.04$ of NGC 2997, the absence of an active nucleus (see Section 4.3), and the observed logarithmic measure of FIR/radio flux density ratio at our observing frequencies show that the linear correlation between FIR and radio emission exists in NGC 2997. For estimating various parameters such as average formation rate of stars more massive than 5 M$_\odot$ [SFR ($M \gtrsim 5$ M$_\odot$) M$_\odot$ yr^{-1}] and the ionization rate of the Lyman continuum photons (s^{-1}) given in Table 7, we assumed a simple model with only one free parameter – the average formation rate of stars more massive than 5 M$_\odot$ (Condon 1992).

Radio counts of young Galactic supernovae remnants (SNRs) suggest a radio supernova rate of 0.013 yr^{-1} (Caswell & Lerche 1979) or the Type II supernova rate $\nu_{SN} \sim 0.023$ yr^{-1} estimated by Tammann (1982). Our data suggest that the supernova rate in NGC 2997 is a factor of 3–4 times higher than that of our Galaxy. The Lyman continuum photon rate of the Galaxy is 2×10^{53} photon s^{-1} (Güsten & Mezger 1982). The derived SFR in NGC 2997 suggest that the galaxy is a normal galaxy with intermediate star formation. The derived values of SFR and the Lyman continuum photon rate of NGC 2997 are less than the values derived for M82 by Condon (1992) but higher than our Galaxy. For M82, the SFR ($M \gtrsim 5$ M$_\odot$) is $\sim$2.2 M$_\odot$ yr^{-1}, the ionization rate is $N_{uv} \sim 8 \times 10^{53}$ s^{-1} and the radio supernova rate is $\nu_{SN} \sim 0.1$ yr^{-1} (Condon 1992).

4.2 Spectral index (SI) distribution

The spectral index ($S_\nu \propto \nu^\alpha$) distribution across the galaxy was determined by using total intensity maps of identical beamsize at 1272 and 332 MHz, respectively. Both the maps were convolved with a circular Gaussian beam of 18 arcsec in size and all points below 3σ level were blanked out. The spectral index map ($\alpha_{1.27,0.33}$) was then derived using the COMB task in AIPS. The SI map between 1272 and 332 MHz is shown as a grey-scale image in Fig. 4 (left)

Table 3. Map parameters.

Figure	1a	1b	1c
Band centre (MHz)†	1272	616	332
Synthesized beam[a]	15.8×12.4 arcsec^2 @25°	17.9×11.7 arcsec^2 @41°	15.9×12.0 arcsec^2 @14°
Restoring beam[b]	15 arcsec	15 arcsec	15 arcsec
UV-taper/weighting	20 kλ/NA	20 kλ/NA	16 kλ/UN
rms noise (mJy beam^{-1})	0.3	0.6	1.0
Figure	2	5-contour	5-left grey[c]
Band centre (GHz)†	1.27	1.27	4.8
Synthesized beam[a]	50.9×36 arcsec^2 @11°	4.06×2 arcsec^2 @11°	1.5×0.7 arcsec^2 @55°
Restoring beam[b]	45 arcsec	3 arcsec	3 arcsec
UV-taper/weighting	5 kλ/NA	None/UN	None/UN
rms noise (mJy beam^{-1})	0.6	0.08	0.04

†All maps are Stokes I and corrected for the shape of the GMRT primary beam.
NA, Natural weighting; UN, Uniform weighting.
Final bandwidth for analysis after editing is about ∼12.5 MHz at each frequency.
[a]Synthesized beam for a deconvolution; position angle with respect to the major axis is given in degrees.
[b]Restoring beam is a circular Gaussian with PA = 0°, and the area is approximated to the deconvolving beam area in arcsec^2, $\Omega_s = 1.13\beta_{maj} \times \beta_{min}$.
[c]Map using the VLA archival data.

Table 4. Some discrete components in the disc of NGC 2997.

Source	Observed position at 1272 MHz α_{2000} = h m s ± s, δ_{2000} = ° ′ ″ ± ″	Integrated flux densities (mJy) and peak intensities (mJy beam^{-1}) at 1272 MHz	616 MHz	332 MHz	Spectral index 332–1272 MHz ($S_\nu \propto \nu^\alpha$)	Comments
1	09 45 38.76 ± 0.0	38.7 ± 1.6	56.6 ± 3.1	86.3 ± 4.0	−0.6	Nuclear region
	−31 11 26.60 ± 0.3	21.0 ± 0.5	28.4 ± 1.2	40.9 ± 1.3	−0.5	
2	09 45 39.65 ± 0.1	13.7 ± 2.4	20.9 ± 4.8	21.0 ± 4.6	−0.31	North source
	−31 08 51.15 ± 2.1	4.2 ± 0.6	6.9 ± 1.2	8.1 ± 1.3	−0.48	
3	09 45 45.05 ± 0.1	16.7 ± 2.1	14.0 ± 4.6	12.04 ± 3.6	0.24	H II region in northern
	−31 10 33.08 ± 1.1	6.0 ± 0.6	4.9 ± 1.2	6.5 ± 1.4	−0.06	arm
3.1	09 45 45.87 ± 0.3	19.3 ± 3.7	27.0 ± 5.2	59.8 ± 14	−0.84	Northern ridge
	−31 10 41.19 ± 2.3	6.3 ± 0.5	6.8 ± 0.9	15.2 ± 1.2		component (∼5.0 by 2.1 kpc)
4	09 45 30.53 ± 0.2	5.3 ± 2.0	18.3 ± 5.6	22.6 ± 4.9	−1.08	Non-thermal north-west
	−31 10 54.90 ± 4.1	2.1 ± 0.6	5.0 ± 1.2	8.0 ± 1.3	−0.98	component
5	09 45 37.42 ± 0.3	6.1 ± 2.1	5.8 ± 3.2	15.6 ± 5.0	−0.69	Component in southern arm
	−31 12 28.48 ± 2.3	2.25 ± 0.5	3.42 ± 1.3	5.4 ± 1.3	−0.65	
6	09 45 48.84 ± 0.2	26.1 ± 4.4	13.3 ± 4.1	22.5 ± 5.3	0.11	East component of
	−31 11 36.10 ± 2.5	3.9 ± 0.5	5.4 ± 1.2	7.3 ± 1.3	−0.45	north-east arm

Table 5. Global radio continuum properties of NGC 2997.

Observing band (MHz) ⟶	332	616	1272
Flux density (mJy)†	1134 ± 111	730 ± 22	367 ± 8
Spectral power (10^{21} W Hz^{-1})	24.4 ± 1.7	15.7 ± 0.3	7.9 ± 0.1
Global spectral index ($S_\nu \propto \nu^\alpha$)	332 → 616 : −0.71	616 → 1272 : −0.94	332 → 1272 : −0.84

†The reasonable error bars in flux density scale are expected to be $\lesssim$10 per cent.

with the 1272-MHz radio contour map superimposed on it. The uncertainty for the measured SI map is shown in the right-hand panel of Fig. 4. The spectral index measured over most of the disc shows uncertainty in the range of 0.05–0.25. The uncertainty map (Fig. 4, right-hand panel) shows intense regions (i.e. high S/N) having error $\lesssim$0.15 whereas uncertainty increases in the fainter parts of the galaxy. Strong features registered with position errors of the order of 3–4 arcsec in total intensity maps can make larger changes in the spectral index measurements. The errors in RA and Dec. in our total intensity maps are $\sim \pm 0\overset{s}{.}22$ and $\sim \pm 2$ arcsec, respectively.

The SI map in Fig. 4 shows that the radio spectrum is flatter in nature wherever brightness peaks such as intense spiral arms and nucleus exist, whereas the radio spectrum of the outer parts of spiral arms show steeper spectrum. The radio emission from normal galaxies is known to be closely related to the population of young massive main-sequence stars which ionizes the H II regions causing the free–free thermal radio emission. The supernova explosions of these young massive stars accelerate the relativistic electrons causing the non-thermal synchrotron emission. As the spectral indices of Galactic SNRs are known to show a broad range ($-0.2 < \alpha < -0.8$) with a mean value of ~ -0.5 (Trushkin 1999) and considering

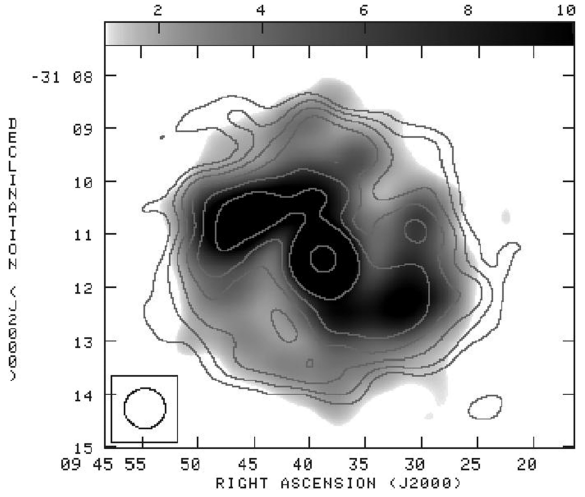

Figure 2. The GMRT 1272-MHz radio contour map of NGC 2997 with a beamsize of 45 arcsec overlaid on the NVSS 1400 MHz grey-scale image (Condon et al. 1998). The disc extent and morphology of the GMRT low-resolution map is similar to the NVSS image indicating that the GMRT map is sensitive to large scales. The rms σ is 0.6 mJy per beam area, contours starting from 3σ level and scaled by a factor of $\sqrt{2}$.

that the thermal fraction of the observed total flux densities at low frequencies is less than 10 per cent, the relative flatter spectral index regions in spiral arms could suggest direct contribution of non-thermal emission by SNRs. The spectral index value which increases up to $\sim -1.2 \pm 0.2$ in the outer parts of the spiral arms indicates the energy losses of the relativistic electrons while they diffuse away out of their place of origin in the star-forming regions.

We measured a spectral index -0.6 ± 0.04 for the nucleus by a single power law fit to the flux densities listed in Table 4 (source 1). This is consistent with the mean spectral index value of the nucleus in the SI map shown in Fig. 4 ($\alpha_{1.27,0.33} \sim -0.62 \pm 0.1$). A relatively flatter spectral index of the nuclear region might be due to a younger population of particles, due to the thermal contribution by ionized gas in massive-star clusters and SNR.

The spatial spectral index for the ridge component in the northern spiral arm varies as $-0.78 \lesssim \alpha_{1.27,0.33} \lesssim -0.46$. The source 3 in the ridge component (Fig. 4, left-hand side) is a giant H II region and the core source in this region is classified as a thermal source (Firpo et al. 2005). The spectral index value for source 3 is ~ -0.06 (see Table 4) and confirms the thermal nature of emission.

4.3 The circumnuclear ring

We detect a strong nuclear source in NGC 2997 at all the wavebands which is resolved into a circumnuclear star-forming ring in our high-resolution 1272 MHz image. NGC 2997 is an intermediate-type SAB(rs)c galaxy with several hotspots. The circumnuclear star-forming ring has been observed in the optical and NIR (Maoz et al. 1996; Elmegreen et al. 1999). Circumnuclear rings are observed in 20 per cent of all spiral galaxies and mostly occur in barred galaxies (Knapen 2005). Observational studies (Allard, Peletier & Knapen 2005; Böker et al. 2008) show that the circumnuclear ring can arise due to the bar-driven radial inflow of magnetized gas materials which get accumulated in a ring near the location of inner Lindbland resonances. There are two models that explain the star formation in circumnuclear rings: (i) in the gravitational instability or 'popcorn' (Elmegreen 1994; Böker et al. 2008) model, star formation is driven by stochastic gravitational fragmentation along the ring where the star-forming regions have a regularly spaced distribution (Elmegreen et al. 1999); (ii) in the 'pearls on a string' model, the gas along the bar that flows into the ring is compressed near the contact points. Star formation is then triggered in these overdensity contact regions. Observationally, an age gradient in the star-forming regions is seen along either half of the ring (Allard et al. 2005; Böker et al. 2008).

We made a high-resolution image at 1.27 GHz using robust weighting of -5 in the task IMAGR. The resulting angular resolution of 3 arcsec ($\sim$200 pc) resolved the circumnuclear ring (see Fig. 5) into five star-forming clumps, i.e. hotspots. We measured the position, peak intensity and integrated flux density of each hotspot by fitting a Gaussian using the task JMFIT in AIPS. The position for each component is listed using seconds for RA and arcsec for Dec. in Table 8. The observed luminosity for the individual hotspot is between 0.16 and 1.58×10^{20} W Hz^{-1} in a 20-cm band with a 200-pc resolution. We also calibrated and imaged the VLA archival data of this galaxy at 4.8 GHz. The resulting image

Table 6. Total flux density measurements of NGC 2997.

Frequency (GHz)	Flux density (Jy)	Reference
8.460	0.034 ± 0.004	Han et al. (1999)[a]
5.010	0.092 ± 0.010	Whiteoak (1970)
4.860	0.067 ± 0.011	Han et al. (1999)[a]
4.850	0.141 ± 0.014	Wright et al. (1996)
2.373	0.160 ± 0.010	Han et al. (1999)
1.543	0.255 ± 0.020	Han et al. (1999)
1.490	0.290	Condon (1987)
1.400	0.235 ± 0.010	Condon et al. (1998)
1.272	0.367 ± 0.008	This paper
0.616	0.730 ± 0.022	This paper
0.332	1.134 ± 0.111	This paper

[a]Lower limits, because of the missing spacing problems, were not included in the fit in Fig. 3.

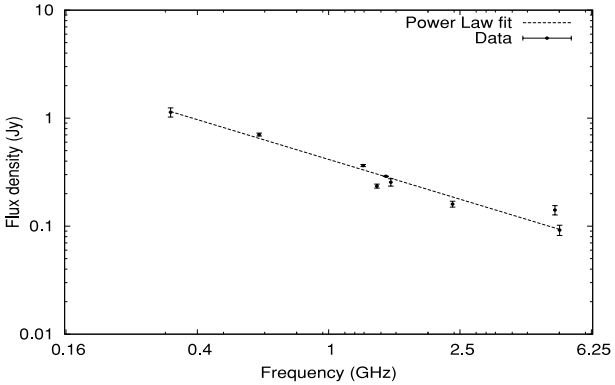

Figure 3. The total emission spectra of NGC 2997. In addition to our three GMRT data points, the data given in Table 6 are also plotted. The dashed line is the best least-squares fit to the data with a power-law index $\alpha = -0.92 \pm 0.04$.

Table 7. Estimated parameters for NGC 2997.

	Disc	Nuclear region
1. Star formation rate ($M_\odot$ yr^{-1})	1.9	0.2
2. The ionization rate (10^{53} s^{-1})	6.7	0.8
3. The supernova rate (yr^{-1})	0.08	0.01

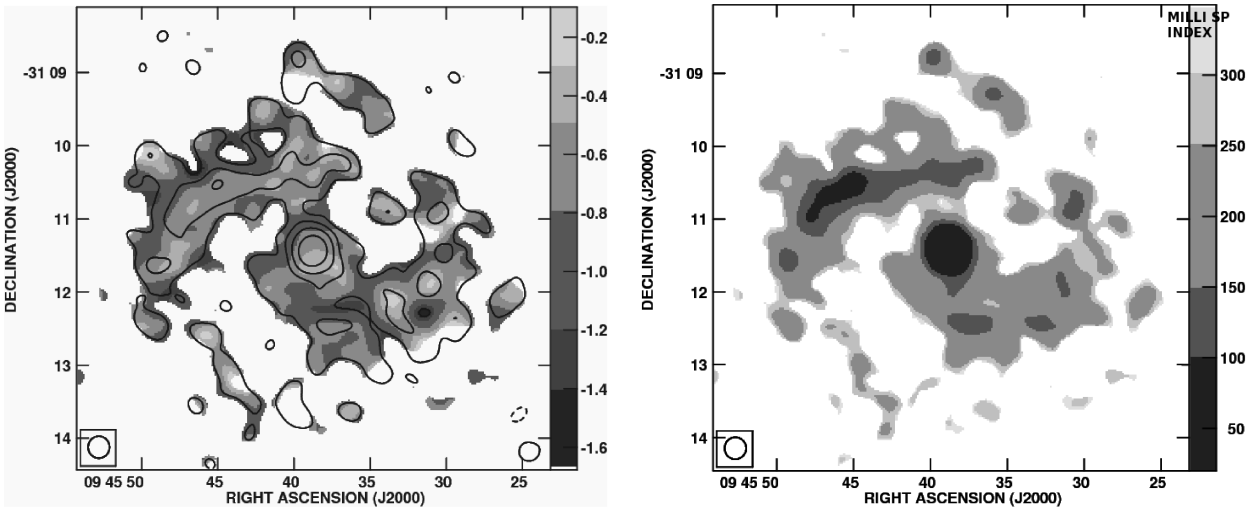

Figure 4. The left-hand panel shows grey-scale spectral index image ($\alpha_{1.27,0.33}$) between 1272 and 332 MHz and the right-hand panel shows the image of spectral index uncertainty. The radio contour map at 1272 MHz superimposed on the grey-scale spectral index image with contours $(-3, 3, 6, 12, 24)\times \sigma$ level. The rms σ is 0.5 mJy per beam area and the nucleus is the brightest region of the galaxy. All the images in this figure are restored with a beamsize of 18 arcsec; the beamsize is indicated at the BLC.

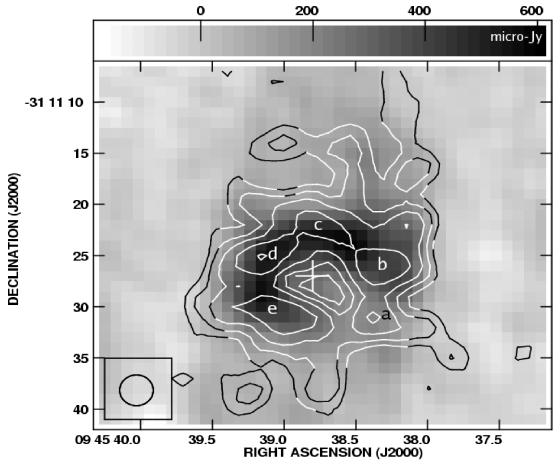

Fig.5 left: Contour levels are at 0.24, 0.4, 0.56, 0.72, 0.88, 1.04, 1.2, 1.36 mJy beam^{-1}, the peak brightness is 1.39 mJy beam^{-1}

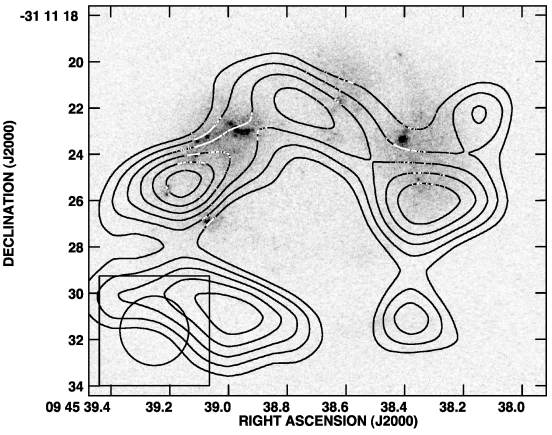

Fig.5 right: Contour levels are at 0.72, 0.84, 0.96, 1.07, 1.2, 1.32 mJy beam^{-1}, the peak brightness is 1.39 mJy beam^{-1}

Figure 5. The GMRT radio contour map of the nuclear region at 1.27 GHz with an angular resolution of 3×3 arcsec^2 overlaid on (left) grey-scale archival VLA 4.8 GHz C-band image (restored with a beamsize of 3×3 arcsec^2, PA $= 0^\circ$) and (right) grey-scale *HST* archival *V*-band 2300-Å image (Courtesy, Maoz et al. (1996); resolution ∼0.05 arcsec, PA $= 84.^\circ30$).

Table 8. Radio hotspots in the circumnuclear region of NGC 2997.

Hotspot	Position (J2000) RA (s), Dec. (arcsec)	Deconvolved angular size (arcsec^2 PA)	Peak intensity (mJy beam^{-1})	Integrated flux density (mJy)	Radio luminosity (10^{20} W Hz^{-1})
a	38.37, 31.01	1.7×1.3 @167°	0.61	0.77 ± 0.17	0.16
b	38.32, 25.77	7.5×5.0 @ 88°	1.34	7.0 ± 0.5	1.52
c	38.78, 22.31	12.5×4.0 @ 76°	0.77	5.0 ± 0.6	1.17
d	39.12, 25.00	7.7×2.1 @122°	0.96	3.27 ± 0.3	0.7
e	39.02, 30.86	9.4×4.0 @71 °	1.34	7.36 ± 0.5	1.58

shown as grey-scale in Fig. 5 (left) also detects the circumnuclear ring coincident with the 1.27 GHz-ring. Fig. 5 (right) shows the 1.27-GHz radio contour map overlaid on *HST V*-band grey-scale image (Maoz et al. 1996). The radio ring is coincident but more extensive than the observed structure of the ring in the *V* band. This is likely to be due to the lower angular resolution at radio wavelengths and partly probably due to extinction at optical wavelengths which Elmegreen et al. (1999) estimate to be about 3 mag in the vicinity of the ring. The morphological structure of the circumnuclear region in our 1.27-GHz radio contour map is similar to the contour maps of relative intensities in the *U* band published by Meaburn & Terrett (1982) using the SAAO 1.9-m reflector.

Our radio contour map and the grey-scale images in the *UV* (2300 Å) and radio (4.8 GHz) band shown in Fig. 5 indicate that there is no detectable radio continuum emission from the central part of the nucleus, confirming that there is no radio-loud AGN at the centre of this galaxy. Maoz et al. (1996) observed circumnuclear rings in five barred or weakly barred spiral galaxies of type Sc (including NGC 2997) and none of the rings hosted an AGN at its centre. The quiescent phase of the nucleus was also noted in the detailed study of the NGC 2997 nucleus by Walsh et al. (1986). A large number of hotspots are observed on a complete circumnuclear ring of NGC 2997 at NIR (Elmegreen et al. 1999) whereas only three northern star-forming regions are visible in the *V*-band image. We note that the intense NIR hotspots located in the northern part of the ring correlate with the radio hotspots. Weak radio emission is detected from the southern parts of the ring although hotspots are not distinguishable. The faint emission along the southern half of the ring is seen in *UV* (Maoz et al. 1996), *U* (Meaburn & Terrett 1982) band image. Faint southern hotspots are also seen in the NIR ring which Elmegreen et al. (1999) attribute to the heavy dust extinction since the southern hotspots are being observed through the dust lanes. A slight offset between the optical and radio positions of the hotspots is observed. This could be attributed to the poor angular resolution of the radio data (∼3 arcsec) as compared to the excellent resolution of the optical data (∼0.05 arcsec) and dust extinction near the star-forming peaks.

The circumnuclear ring that we detect in radio has a deconvolved diameter of 11.6 ± 0.08 arcsec i.e. ∼750 pc. The separation between the hotspots ranges from ∼190 to 370 pc. This is comparable to the NIR where the diameter of the ring is ∼570 pc (∼8.7 arcsec) and the spacings between hotspots is ∼200 pc (Elmegreen et al. 1999). This is typical of the circumnuclear rings detected in other galaxies. The average size of the nucleus from the photometric and morphological analysis of the galaxies with peculiar nuclei is quoted to be less than 800 pc (Pastoriza 1975).

We compared the circumnuclear ring (CNR) in NGC 2997 to the well-studied CNR in NGC 1097 (Walsh et al. 1986; Barth et al. 1995; Beck et al. 1999; Sandstrom et al. 2010). The CNR of NGC 1097 has ∼1.5 kpc diameter (Beck et al. 2005) and a LINER/Seyfert 1 AGN at its centre. Three prominent radio hotspots are seen at 3.5 cm in NGC 1097 (Beck et al. 2005) whereas four bright and one faint hotspots are observed in NGC 2997 at 20 cm (see Fig. 5). No azimuthal age gradient is seen in massive stars of both the rings with ages less than 10^7–10^8 yr (Maoz et al. 1996; Elmegreen et al. 1999; Sandstrom et al. 2010) and both rings show regular distribution of hotspots (Barth et al. 1995; Elmegreen et al. 1999; Beck et al. 2005) which lends support to the gravitational instability model (Elmegreen 1994) for the star formation in the CNR. The CNR in NGC 1097 is formed due to the gas driven by bar potential. Various observational studies show that NGC 2997 does not possess either a prominent large-scale bar or an active nucleus (Walsh et al. 1986; Maoz et al. 1996), hence unlike NGC 1097 gas accumulation in the CNR of NGC 2997 is unclear. However, fast magnetohydrodynamic density waves (FMDWs) at the modified inner Lindbland resonance (mILR) model (Lou et al. 2002; Lou 2003) can explain the formation of CNR in NGC 2997.

We estimate an equipartition field in the central nuclear region of diameter ∼750 pc to be about 30 μG. This is similar to the field strength of 34 μG estimated by Han et al. (1999) for the central region of NGC 2997 and 40 μG estimated for the CNR in NGC 1097 by Beck et al. (1999). The equipartition field for the radio hotspots in NGC 2997 ranges from ∼30 to 50 μG. We estimate a disc field of ∼4 μG for NGC 2997.

We compared the luminosity of radio hotspots in circumnuclear region of NGC 2997 with the circumnuclear radio hotspots in other galaxies such as NGC 253, 1365 and 1808. NGC 253 is a nearby ($d \sim 2.5$ Mpc) starburst galaxy, in which Ulvestad (2000) detected 22 compact circumnuclear sources at 20 cm with ∼28 pc resolution. The detected circumnuclear sources of NGC 253 have a typical radio power of 2×10^{18} W Hz^{-1}. Stevens, Forbes & Norris (1999) detected seven hotspots in the circumnuclear region of NGC 1365 at 3 and 6 cm with a 100 pc resolution ($d \sim 20$ Mpc). The luminosity of circumnuclear hotspots for NGC 1365 at 20 cm (derived using a SI from 6 and 3 cm) ranges from ∼0.8 to 2×10^{20} W Hz^{-1}. Similarly, Collison et al. (1994) detected hotspots in NGC 1808 with a resolution of 98 pc. The luminosity of circumnuclear hotspots in NGC 1808 ($d \sim 9.9$ Mpc) at 20 cm (derived using an SI between 6 and 3.6 cm) ranges from ∼0.2 to 3.8×10^{20} W Hz^{-1}. Thus, the average luminosity of hotspots in a CNR observed with ∼100 pc resolution appears to be 10^{19} to a few times 10^{20} W Hz^{-1} at 20 cm. It is likely that the hotspots are composed of several 2×10^{18} W Hz^{-1} clumps as seen in NGC 253 in addition to a diffuse non-thermal emission. Assuming that the observed emission at 1.27 GHz from the circumnuclear hotspots is mostly non-thermal in nature, we derived the SN rate based on the Condon & Yin (1990) equation. The median SN rate value for the discrete components in NGC 2997 ring is ∼0.001 yr^{-1}. The median value of the average formation rate of stars [SFR ($M \geq 5\,M_\odot$) $M_\odot$ yr^{-1}] estimated for the hotspots is ∼0.024 $M_\odot$ yr^{-1}.

The spectral index $\alpha_{4.8,1.27}$ of the CNR in NGC 2997 is $\sim -0.64 \pm 0.1$. We could not estimate the spectral index of the individual hotspots since these were not clearly discernible in the convolved 4.8-GHz map (see Fig. 5). NGC 6951, unlike NGC 2997, hosts a central AGN and has a marginally larger diameter (∼1 kpc) of the CNR but both the rings show hotspots that form an almost complete ring. In NGC 2997, the radio ring is fainter to the south whereas in NGC 6951 the ring appears to be broken in the north and south (Saikia et al. 2002). The spectral index of the circumnuclear emission in NGC 6951 between 20 and 6 cm was found to be −0.84 (Ho & Ulvestad 2001). The radio spectrum of the hotspots in the CNR of other galaxies exhibits a large range in spectral index. For example, the CNR in NGC 613 has a spectral index of −0.65 between 2 and 6 cm (Hummel & Jörsäter 1992) similar to NGC 2997, whereas the spectral index of the individual compact sources (total 19) in the CNR of NGC 4736 exhibits a spectral index ranging from 0.1 to −0.8 between 6 and 20 cm (Duric & Dittmar 1988). A similar kind of distribution is also noted in the CNR of NGC 1365 between 3 and 6 cm by Stevens et al. (1999). Out of the seven hotspots detected in the ring of NGC 1365, four show a steep spectrum and the rest show a flat spectrum with the spectral index ranging from 0.04 to −0.4 (Stevens et al. 1999). Stevens et al. (1999) attribute synchrotron emission from hotspots to electrons accelerated by SN and SNRs. The spectral indices of circumnuclear hotspots detected between 3.6 and 6 cm in NGC 1808 (Collison et al. 1994) are also consistent with their being dominated by SNRs. Utilizing a *V*-band *HST* exposure of NGC 2997, Maoz et al. (1996) determined the numerous compact (few pc radius) sources distributed along the ring that are probably young (less than 10^8 yr) and massive (∼10^5 $M_\odot$) clusters of stars that are gravitationally bound.

5 SUMMARY

We have presented high-resolution radio continuum maps of NGC 2997 at 332, 616 and 1272 MHz. To the best of our knowledge

these are the first images of the galaxy at $\nu < 1.4$ GHz. The radio continuum features detected in our observation bands are described, in detail, along with the spectral index values. The best-fitting single power law model to the integrated radio spectrum of NGC 2997 gives a spectral index $\alpha = -0.92 \pm 0.04$. The best-fitting value of $\alpha = -0.79 \pm 0.07$ obtained using only the low-frequency GMRT data suggests a break in the spectrum at $\nu < 1$ GHz. We put an upper limit of 10 per cent on the thermal fraction at 1 GHz.

The spectral power of NGC 2997 at our observing frequencies is in the range of 7.9 to 24.4×10^{21} W Hz^{-1}. The derived logarithmic measure of FIR/radio flux density ratio, $\hat{q}_{\rm FIR}$ parameter is $\sim 2.19 \pm 0.03$, which is near the median for spiral galaxies at 1.4 GHz, $\hat{q}_{\rm FIR} \approx 2.30$ (Condon 1992). The estimated values for average SFR ($M \gtrsim 5\,{\rm M}_{\odot}$) is 1.9 M$_{\odot}$ yr^{-1}, the supernovae rate is 0.08 yr^{-1}, and the production rate of the Lyman continuum photons is 6.7×10^{53} s^{-1}. The resultant logarithmic measure of FIR/radio flux density ratio and the intermediate average SFR confirms that NGC 2997 is a normal galaxy.

The low-frequency spectral index distribution map ($\alpha_{1.27,0.33}$) of NGC 2997 shows that the radio spectrum is flatter in nature near brightness peaks such as in the intense spiral arm regions and nucleus, whereas the radio emission from the low surface brightness regions shows a steeper spectrum. The measured spectral index for the nucleus between 332 and 1272 MHz is $\alpha \sim -0.6 \pm 0.04$.

The radio continuum map at 1272 MHz with an angular resolution of 3 arcsec ($\sim$200 pc) reveals a circumnuclear ring structure with five radio hotspots. No radio continuum emission at the centre of the galaxy is detected indicating that there is no radio-loud AGN. Part of the ring to the south is faint. The circumnuclear ring is similar to that observed at other wavebands from the galaxy and in other galaxies. It has a deconvolved diameter of $\sim$750 pc and the separation between hotspots range from $\sim$190 to 370 pc. We estimate an equipartition field in the central nuclear region of diameter $\sim$750 pc to be about 30 μG. The observed luminosity for the individual hotspot is about 10^{20} W Hz^{-1}. The median SN rate and the average formation rate of stars, SFR ($M \gtrsim 5\,{\rm M}_{\odot}$), for the hotspots in the ring are 0.001 yr^{-1} and 0.024 M$_{\odot}$ yr^{-1}, respectively.

ACKNOWLEDGMENTS

We thank the staff of the GMRT who have made these observations possible. GMRT is run by the National Centre for Radio Astrophysics of the Tata Institute of Fundamental Research. We thank the anonymous referee for useful comments on the manuscript. JK thanks the Dean of the GMRT, Prof. Y. Gupta, for his support. One of the authors (SA) wishes to thank R. Wielebinski for bringing to his notice the importance of low-frequency observation of NGC 2997. This research has made use of the NASA/IPAC Extragalactic Data base which is operated by the Jet Propulsion Laboratory, Caltech under contract with the NASA.

REFERENCES

Allard E. L., Peletier R. F., Knapen J. H., 2005, ApJ, 633, L25
Ananthakrishnan S., 2005, Proc. 29th Int. Cosmic Ray Conf., Pune, 10, 125
Barth A. J., Ho L. C., Filippenko A. V., Sargent W. L., 1995, AJ, 110, 1009
Beck R., Ehle M., Shoutenkov V., Shukurov A., Sokoloff D., 1999, Nat, 397, 324
Beck R., Ehle M., Fletcher A., Harnett J., Shoutenkov V., Shukurov A., Sokoloff D., 2005, AIP Conf. Proc., 783, 216
Böker T., Falcón-Barroso J., Schinnerer E., Knapen J. H., Ryder S., 2008, AJ, 135, 479
Caswell J. L., Lerche I., 1979, MNRAS, 187, 201
Collison P. M., Saikia D. J., Pedlar A., Axon D. J., Unger S. W., 1994, MNRAS, 268, 203
Condon J. J., 1987, A&AS, 65, 485
Condon J. J., 1992, ARA&A, 30, 575
Condon J. J., Broderick J. J., 1988, AJ, 96, 30
Condon J. J., Yin Q. F., 1990, ApJ, 357, 97
Condon J. J., Frayer D. T., Broderick J. J., 1991, AJ, 101, 362
Condon J. J., Cotton W. D., Greisen E. W., Yin Q. F., Perley R. A., Taylor G. B., Broderick J. J., 1998, AJ, 115, 1693
de Vaucouleurs G., de Vaucouleurs A., Corwin J. R. H. G., Buta R. J., Paturel G., Fouque P., 1991, Third Reference Catalogue of Bright Galaxies. Springer, New York
Duric N., Dittmar M. R., 1988, ApJ, 332, L67
Elmegreen G. B., 1994, ApJ, 425, L73
Elmegreen D. M., Chromey F. R., Sawyer J. E., Reinfeld E. L., 1999, AJ, 118, 777
Firpo V., Bosch G., Morrell N., 2005, MNRAS, 356, 1357
Fitt A. J., Howarth N. A., Alexander P., Lasend A. N., 1992, MNRAS, 255, 146
Garcia A. M., 1993, VizieR Online Data Catalog, 410, 47
Grosbøl P., Dottori H., Gredel R., 2006, A&A, 453, L25
Güsten R., Mezger P. G., 1982, Vistas Astron., 26, 159
Han J. L., Beck R., Ehle M., Hynes R. F., Wielebinski R., 1999, A&A, 348, 405
Helou G., Soifer B. T., Rowan-Robinson M., 1985, ApJ, 298, L7
Ho L. C., Ulvestad J. S., 2001, ApJS, 133, 77
Hummel E., 1991, A&A, 251, 442
Hummel E., Jörsäter S., 1992, A&A, 261, 85
Israel F. P., Mahoney M. J., 1990, ApJ, 352, 30
Kennicutt R., 1983b, A&A, 120, 219
Knapen J. H., 2005, A&A, 429, 141
Koribalski B. S. et al., 2004, AJ, 128, 16
Lacki B. C., Thompson T. A., Quataert E., 2010, ApJ, 717, 1
Lou Y. Q., 2003, Acta Astron. Sinica, 44, 172
Lou Y. Q., Walsh W. M., Han J. L., Fan Z., 2002, ApJ, 567, 289
Maoz D., Barth A. J., Sternberg A., Filippenko A. V., Ho L. C., Macchetto F. D., Rix H.-W., Schneider D. P., 1996, AJ, 111, 2248
Meaburn J., Terrett D. L., 1982, MNRAS, 200, 1
Men H., Han J. L., 2005, Chinese J. Astron. Astrophys., 5, 49
Milliard B., Marcelin M., 1981, A&A, 95, 59
Niklas S., Klein U., Wielebinski R., 1997, A&A, 322, 19
Pastoriza M. G., 1975, Ap&SS, 33, 173p
Peterson C. J., 1978, ApJ, 226, 75
Pohl M., Schlickeiser R., Hummel E., 1991, A&A, 250, 302
Roy A. L., Norris R. P., Kesteven M. J., Troup E. R., Reynolds J. E., 1998, MNRAS, 301, 1019
Saikia D. J., Phookun B., Pedlar A., Kohno K., 2002, A&A, 383, 98
Sandstrom K. et al., 2010, A&A, 518, L59
Stevens I. R., Forbes D. A., Norris R. P., 1999, MNRAS, 306, 479
Swarup G., Ananthakrishnan S., Kapahi V. K., Rao A. P., Subrahmanya C. R., Kulkarni V. K., 1991, Curr. Sci., 60, 95
Tabatabaei F. S., Beck R., Krügel, Krause M., Berkhuijsen E. M., Gordon K. D., Menten K. M., 2007b, A&A, 475, 133
Tammann G. A., 1982, in Rees M. J., Stoneham R. J., eds, Supernovae: A Survey of Current Research. p. 371
Trushkin S. A., 1999, Odessa Astron. Publ., 12, 144
Tully R. B., 1988, Nearby Galaxies Catalog. Cambridge Univ. Press, Cambridge
Ulvestad J. S., 2000, AJ, 120, 278
Walsh J. R., Nandy K., Thompson G. I., Meaburn J., 1986, MNRAS, 220, 453
Whiteoak J. B., 1970, Astrophys. Lett., 5, 29
Wright A. E., Griffith M. R., Hunt A. J., Troup E., Burke B. F., Ekers R. D., 1996, ApJS, 103, 145W

This paper has been typeset from a TEX/LATEX file prepared by the author.